Journal of Engineering and Technology for Industrial Applications

ITEGAM-JETIA

Manaus, v.12 n.57, p. 244-258. January/February, 2026.

DOI: https://doi.org/10.5935/jetia. v12i57.2877

ISSN ONLINE: 2447-0228

RESEARCH ARTICLE OPEN ACCESS

PERFORMANCE AND EMISSION ENHANCEMENT OF A CRDI VCR ENGINE FUELED WITH TIO₂-INFUSED TOMATO SEED BIODIESEL USING RSM OPTIMIZATION

Kumaran P[1]*, Sathiyaraj S[2], Vijayakumar K[3], Albinraj[4] and Esakki mani K[5]

[1, 2, 3,4,5]Department Mechanical Engineering, Aarupadai Veedu Institute of Technology, Vinayaka Mission's Research Foundation(deemed to be university), Salem, Tamilnadu, India.

[1]http://orcid.org/ 0000-0003-2781-8999, [2]http://orcid.org/0000-0001-8504-0412, [3]http://orcid.org/0000-0002-5964-982X
[4]http://orcid.org/0009-0003-7581-738X, [5]http://orcid.org/0009-0006-4366-9478

Email: *kumaranp@avit.ac.in, sathiyaraj@avit.ac.in, vijayakumar@avit.ac.in, albinjith94@gmail.com, shivasabari59@gmail.com

ARTICLE INFO

Article History
Received: October 31, 2025
Revised: November 20, 2025
Accepted: January 1, 2026
Published: January 31, 2026

Keywords:
CRDI engine,
Response surface methodology,
Optimization,
Alternative fuels,
Tomato seed biodiesel

ABSTRACT

This study enhanced the response of a CRDI single-cylinder four-stroke VCR engine under various input parameters with a novel tomato seed biodiesel (B25) infused with TiO2 nanoparticles. Response surface methodology (RSM) was employed to examine the influence of various input parameters on engine responses, including specific fuel consumption (SFC), brake thermal efficiency (BTE), and emissions of CO, HC, and NOx. The examined factors included injection pressure (IP), load, compression ratio (CR), and nanoparticle concentration as gasoline additives. Through the optimization of all input parameters, the RSM identified the optimal point at which the engine achieved maximum performance with minimal emissions. The optimal settings for the input parameters are as follows: a nano biofuel mix ratio, an injection pressure of 799 bar, a compression ratio of 20, and a load of 3.63 kg. This configuration of input parameters produces optimal outcomes for BTE (22.46%), SFC (0.25 kg/kWh), CO (0.023%), HC (22.01 ppm), and NOx (536 ppm). To ensure validity, we compared the experimental value with the ideal value predicted by RSM and observed a satisfactory correlation.

1. INTRODUCTION

Biodiesel offers a renewable and cleaner alternative to conventional diesel, yet its performance in modern engines can be limited by factors such as fuel properties and combustion efficiency. Nanotechnology-based additives and advanced fuel systems have emerged as effective solutions to enhance engine output, fuel economy, and emission profiles. Common Rail Direct Injection (CRDI) technology enables precise control over injection parameters, facilitating optimal combustion. This study employs Response Surface Methodology (RSM) to systematically optimize performance and emission characteristics in diesel engines. Authors investigated the use of pulsed electric field (PEF) as a pre-extraction step to enhance TSO yield and quality. Optimum parameters were 9 min treatment and 0.5 µs pulse duration, resulting in maximum extraction of bioactives. Lycopene (565.54 mg/mL) was the main carotenoid, linoleic acid the predominant fatty acid; strong antioxidant activity contributed to high oxidative stability confirmed by EPR and DSC [1]. Authors studied supercritical CO_2 extraction (SFE) of lycopene from tomato pomace, analyzing lycopene concentration and E:Z isomer ratios. Initial process achieved 84.6% lycopene extraction but only 48.4% recovery in oil. Redesign using 703 g of exogenous tomato oil increased predicted lycopene recovery to 99.3%, showing that solubilization efficiency is driven largely by oil availability [2]. Review article summarizing extraction methods, physicochemical characteristics, and bioactive profile of TSO. Highlighted high levels of oleic and linoleic acids, potent antioxidant and antimicrobial properties, and applications in food products, packaging films, dietary supplements, and medical fields. Stressed potential for TSO to add economic value to tomato processing by-products [3].

Compared microwave-assisted extraction (MAE) and supercritical CO_2 extraction (SFE-CO_2) of TSO, optimizing via response surface methodology (RSM). MAE (56.2 °C, 29 min, 67.6 mL) produced higher yield (25.3 wt%) than SFE-CO_2 (16.9 wt%), with similar

fatty acid profiles (~80% unsaturated). γ-Tocopherol was dominant, linked to high DPPH• radical scavenging activity, suggesting strong potential for nutritional and food applications [4]. Researchers examined diesel–tomato seed oil biodiesel (TSOB) blends in a 4-cylinder, 4-stroke, indirect injection diesel engine using both experiments and AVL FIRE CFD simulation. Tested parameters included torque, BSFC, EGT, NOx, CO, CO_2, PM, in-cylinder pressure and temperature, and reaction progress at 1200–2400 rpm. B10 showed the lowest BSFC and B20 the highest torque. CFD revealed NOx formed mainly near the piston throat, CO/CO_2 near chamber boundaries, and PM at the injection region [5]. Researchers developed thiol-grafted Tamarindus indica seed gum–Teff hay biocarbon (TH@TI-TBC) adsorbent for cadmium removal from electroplating wastewater and achieved max adsorption (261.47 mg/g) at pH 5.5, following Langmuir and pseudo-second-order kinetics. Removed 89% of Cd from 30 mg/L wastewater; adsorption driven by electrostatic interaction and surface complexation. Authors proposed TH@TI-TBC as a sustainable waste-to-resource adsorbent [6]. Authors studied acetic acid–treated Pithecellobium dulce seed pod powder for Reactive Red 195-A dye removal. Characterized via SEM, FTIR, DTA, TGA; adsorption followed Temkin isotherm and pseudo-second-order kinetics ($R^2 > 0.90$).

Process was spontaneous and endothermic, suggesting PD pods as low-cost, eco-friendly adsorbents [7]. Researchers extracted 21.69% oil from Rio Grande tomato seeds via Soxhlet (79.83% unsaturated fatty acids), then recovered phenolics from defatted seeds via MAE optimized by RSM (700 W, 70 s, water). Combined oil and phenolic extraction added economic value to tomato waste, producing edible, biofuel, and cosmetic-grade oil and antioxidant-rich extracts through a green, low-cost process [8]. Authors studied turbocharger effects on a VCR diesel engine using neat diesel and neat TSO biodiesel. Turbocharging improved brake thermal efficiency and reduced CO and HC emissions for TSO compared to naturally aspirated operation, but NOx increased without turbo. With turbocharger, NOx emissions for TSO decreased relative to non-turbo TSO operation [9]. Researchers investigated nozzle hole number (2-hole vs 3-hole, 0.25 mm dia) on a single-cylinder DI diesel engine using diesel and B20 TSO at 1500 rpm, 200 bar injection pressure. The 3-hole nozzle improved brake thermal efficiency and reduced SFC at 40% load with B20, and produced lower NOx emissions than the 2-hole nozzle configuration [10]. The biodiesel combustion (apricot, papaya, sunflower, tomato seed oils) at compression ratios 15.5–18.5 in a Kirloskar AV1 diesel engine were simulated using ANSYS Fluent. Higher CR increased peak temperature, pressure, CO_2 and NO, and reduced CO

Apricot biodiesel at CR 18.5 achieved highest combustion efficiency but high emissions; tomato seed oil biodiesel at CR 15.5 showed lowest NO and CO_2 but reduce the performance [11]. Researchers reviewed tomato processing by-products (peels, seeds, pomace) as sources of bioactive compounds (carotenoids, proteins, fiber, pectin) and highlighted tomato seed oil's oxidative stability from carotenoid content and its applicability in food, feed, and biodiesel. The re-use of tomato residues in bakery products, animal feed, meat additives, and non-food industrial applications were analysed [12]. The biodiesel production from tomato seed oil (TSO) using Aspen Plus® were modeled, focusing on alternative catalysts and by-product recovery (glycerol, potassium phosphate). The methyl ester yield correlations and simulated transesterification with methanol recovery and recycle were developed. Designed distillation towers and calculated energy return on investment (EROI), including harvesting and processing energy. Results indicated TSO biodiesel production is technically and energetically feasible [13]. Diesel–TSOB blends were analyzed in an indirect injection (IDI) diesel engine through experiments and 2D CFD (AVL FIRE). CP and combustion characteristics were measured at five loads and seven speeds. B10 at full load had peak CP of 69 MPa at 2200 rpm shows highest accumulative heat release (~1900 J), and best fuel energy efficiency. CFD showed B5 had longest jet penetration (44 mm), while B10 reached peak in-cylinder temperature (1600 K) [14]. Ultrasound-assisted protein extraction from defatted tomato seed cake was optimized using RSM.

The optimum (52 mL/g, 2 min 18 s, 60 min) achieved 35.75% protein yield. The extracted protein exhibited favorable physicochemical properties suitable for food industry applications [15]. Cold press extraction (12.80% yield) and enzyme-assisted aqueous extraction (9.66% yield) for tomato seed oil was analyzed. Both eco-friendly methods preserved oil quality and bioactivity, highlighting their potential for functional food and nutraceutical applications [16]. A UiO-66-NH_2/ZnO/TiO_2 nanocatalyst via sol–gel for biodiesel production was developed from dairy waste scum oil (DWSO). It exhibited a high surface area (568.1 m^2/g) and small particle size (28.35 nm). Using CCD optimization, a 98.7% conversion was achieved at a 9.8:1 methanol/oil ratio, 61 °C, and 2 wt% catalyst [17]. Diesel engine performance was optimized using ternary blends of n-heptane, biodiesel, and diesel with TiO_2 nanoparticles (0–75 ppm) under varying loads, employing RSM. Optimum at 76.8% load, 57.6 ppm NPs, 25.6% biodiesel, and 9.5% n-heptane achieved 77.54 bar CP, 64.65 kJ HRR, 35.12% BTE, and reduced CO (0.0647% vol), HC (52.11 ppm), and smoke (37.34%). Validation errors were <5% [18]. Researchers compared the experimental and ANN-based predictions for CI engine parameters with mahua biodiesel (M30) and 50 ppm of CeO_2, CuO, or TiO_2 NPs. CeO_2 NP blend improved BTE by 9.1%, CP by 11.3%, HRR by 10.2%, and reduced BSFC by 13.7%, CO by 30.4%, HC by 30.1%, smoke by 34.7%, and NOx by 7.1%.

ANN backpropagation with two inputs (load, blend type) effectively predicted performance and emissions, enabling optimal blend selection without extensive testing [19]. Synthesized $ZnFe_2O_4$@TiO_2 nanocatalyst for biodiesel production from jojoba oil, achieving 97.56% yield at 54.96 °C, 2.89% catalyst, and 12.13 mol/mol methanol/oil ratio. Catalyst retained >90% yield after seven cycles. Engine tests showed reduced CO, NOx, and UHC, along with improved BTE and BSFC. Reaction was endothermic ($\Delta H° = 44.82$ kJ/mol) [20]. Biodiesel from a mix of Ceiba pentandra, Mahua longifolia, and Azadirachta indica oils were produced and enhanced with CaO–TiO_2 nano-additives. Optimization by Box–Behnken Design, Deep Belief Network (DBN), and hybrid Arithmetic Optimization was performed. Algorithm identified optimal conditions (load 60%, biodiesel 25%, nano-additive 20 wt%, 1400 rpm). Compared to diesel, CaO–TiO_2 biodiesel reduced BSFC by 41%, CO by 32%, NOx by 25%, and increased BTE by 16.9% [21]. The previous studies examined the individual variables such as biodiesel addition, nanoparticle concentration fluctuations, injection pressure, and compression ratios, additional research into their combined impact is necessary. The author discovered research focused on improving biodiesel volume for engines through the manipulation of compression ratio, load, injection pressure, and nanoparticle concentration.

Therefore, studies that separately control fuel process parameters while jointly managing engine parameters may gain from the present research. Consequently, RSM has been investigated in this study to enhance engine performance and emission metrics. The optimal parameters for operation include nanoparticle concentration, load, CR, and IP. This study involved the incorporation of TiO2 nanoparticles into biodiesel derived from tomato seeds. The engine compression ratio was altered from 18 to 20 in increments of 0.5, the injection pressure was increased from 600 bar to 800 bar in 50 bar increments, and the volume fraction of the biodiesel blend was set at 25%. The concentration of TiO2 nanoparticles was modified in increments of 20 ppm, reaching a maximum of 80 ppm. We employed 2-kilogram increments to adjust the load from 0 to 8 kilograms.

II. MATERIALS AND METHODS

II.1 BIOFUEL PREPARATION PROCESS

We procured the tomato seed oil from the local market in Chennai, Tamil Nadu, India. The subsequent step involved performing the fuel test. Fuel testing indicates that the oil's elevated viscosity renders it unsuitable for direct application in a diesel engine. The objective of the transesterification procedure was to reduce viscosity. The synthesis of biofuels using transesterification is a recognized technique. Subsequently, the mixture was exposed to temperatures between 60 and 70°C in the presence of a suitable catalyst of KOH (1% w/w). The flask was subjected to magnetic stirring at 400 rpm with the mixture. After one hour, a substantial layer had developed in the flask. Following a duration of two hours, the glycerol was isolated by the sedimentation process. B25 is a biofuel mixture including tomato seed oil. The Physio-chemical characteristics of the developed nanofuel is given in table 1.

Table 1: Physio-chemical characteristics of the developed nanofuel.

Oil	Kinematic viscosity (mm^2/s) at 40°C	Density (g/m^3)	High calorific value (kJ/kg)
Tomato seed oil	51.80	917	36,250
Supporting biodiesel B25 (TSO-25%	2.5120	0.8180	40,420
B25+20PPM(TiO_2)	2.6850	0.8235	40,570
B25+40PPM(TiO_2)	2.7105	0.8332	40,810
B25+60PPM(TiO_2)	2.7380	0.8431	41,030
B25+80PPM(TiO_2)	2.8995	0.8795	41,280

Source: Authors, (2026).

II.2 PREPARATION OF NANO-BIODIESEL BLEND

Table 2: Rroperties of TiO2 nanoparticle.

Appearance		Safety related information		Toxicological information	
Form	Fine powder	Boiling point	2972 °C	Inhalation	Avoid inhalation of dust; may cause mild respiratory irritation
		Melting point	1843 °C	Toxicity	Generally considered non-toxic, but nanoparticles may pose inhalation risk
Adour	Odorless	pH	Insoluble in water	-	-
Color	White	Flash Point	N/A	-	-

Source: Authors, (2026).

Table 2 presents the physicochemical parameters of the nanoparticles. The XRD technique is favored for the direct analysis of nanoparticle sample characteristics, including composition size, crystal structure, morphology, purity, and unit dimensions. The subsequent stage involved employing an ultrasonicator to disperse TiO2 nano powder in B25 at different concentrations (20, 40, 60, 80 ppm). Nanoparticles are incrementally added to B25 at consistent intervals for each sample to prevent micromolecule aggregation. Following one hour of high-frequency operation, the Ultrasonicator has completely dissolved all homogenous nanoparticles in the liquid. Consequently, four novel nano-biodiesel blends have been created, comprising 20 PPM (TiO2), 40 PPM (TiO2), 60 PPM (TiO2), and 80 PPM (TiO2) Titanium dioxide.

III. EXPERIMENTAL SET-UP AND METHODOLOGY

III.1 THE SPECIFICATION OF THE EXPERIMENTAL SETUP

This study utilized a CRDI VCR, a single-cylinder diesel engine. The schematic diagram is shown in figure 2. Table 3 presents the specification.

Table 3: CRDI VCR diesel engine specification.

Engine	Model	No. of cylinder	No. of stroke	Orifice diameter	Power	Speed	IP	CR range
Diesel	CRDI VCR	1	4	20 mm	3.5 kW	1500 rpm	60 MPa	12:1 to 18 :1

Source: Authors, (2026).

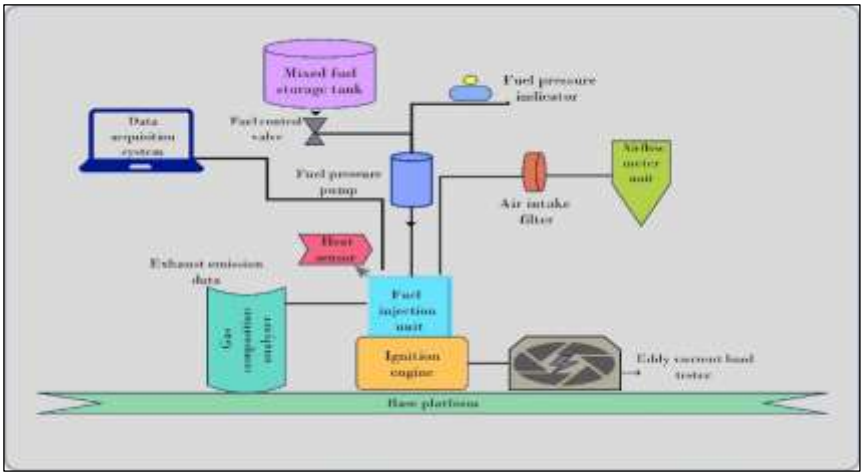

Figure 2: Block diagram of CRDI VCR engine.
Source: Authors, (2026).

III.2 RSM MODELING

III.2.1 Statistical analysis of response surface methodology

Table 4: Factors and Levels of input factors.

Input parameters	Coded levels					
	Symbol	-2	-1	0	1	2
A: Fuel	ppm	B25 (0)	B25 + 0.2 TiO_2 (20)	B25 + 0.4 TiO_2 (40)	B25 + 0.6 TiO_2 (60)	B25 + 0.8 TiO_2 (80)
B: LOAD	kg	0	2	4	6	8
C: IP	bar	600	650	700	750	800
D: CR	-	18	18.5	19	19.5	20

Source: Authors, (2026).

RSM is a data-centric methodology that enhances the output variable, influenced by several independent factors, by selecting the regression model based on quantitative data from the associated study. Response surface methodology is utilized to identify nonlinear interactions between inputs and outputs. Table 4 presents the optimal and non-optimal values of the input parameters corresponding to the -2, -1, Centre (0), +1, and +2 numerical values in this optimization study, as determined by statistical analysis. The objective of the central composite rotational design (CCRD) is to identify the optimal values for the input parameters and their interrelationships. Table 5 presents the experimental configuration for the CCRD design. While the Taguchi technique and factorial design are not ideally suited for optimizing nonlinear systems, they can do so effectively. Response surface methodology establishes a numerical relationship that encompasses the interactions between input parameters and output responses, which is challenging to achieve using optimization techniques; this constitutes the primary advantage of its application in the present study. In optimization approaches, it is essential to ascertain the relationship between input variables and output variables.

Table 5: Experimental array.

Run	A: Fuel (TiO_2 concentration)	B: LOAD	C: IP	D: CR	BTE (%)	SFC (kg/kWh)	CO (%)	HC (ppm)	NO_x (ppm)
1	60	6	750	19.5	30.95	0.432	0.0377	35.42	648
2	40	4	700	19	25.21	0.536	0.0501	27.93	388
3	40	4	700	19	25.4	0.541	0.0504	28.12	389
4	40	4	800	19	25.48	0.502	0.0373	24.56	512
5	60	2	750	18.5	19.95	0.6957	0.057	20.71	310
6	20	2	750	18.5	18.65	0.7507	0.0608	17.4	296
7	60	6	750	18.5	30.68	0.4317	0.0392	34.94	601
8	20	2	650	19.5	18.57	0.7611	0.0622	20.99	226
9	20	2	750	18.5	18.64	0.7507	0.0608	17.4	296
10	40	4	700	18	24.88	0.5478	0.0513	27.38	347
11	40	4	700	19	25.21	0.536	0.0501	27.93	388
12	40	4	600	19	24.24	0.568	0.0532	30.92	301
13	20	6	650	19.5	28.45	0.5261	0.0444	35.22	505
14	40	4	700	19	25.21	0.536	0.0501	27.93	388
15	40	4	700	18	25.54	0.5215	0.0489	28.64	437
16	80	6	650	18.5	30.37	0.4847	0.0424	38.24	485
17	20	6	750	19.5	28.75	0.4979	0.0415	31.99	612
18	0	4	700	19	22.07	0.601	0.0543	25.2	364
19	20	6	750	18.5	28.45	0.5107	0.0427	31.44	574
20	40	0	700	19	5.03	0.696	0.0672	14.36	163
21	40	8	700	19	32.24	0.511	0.0429	46.82	799
22	20	2	750	19.5	18.75	0.532	0.0587	17.62	341

23	40	4	700	19	25.21	0.536	0.0501	27.93	388
24	40	4	700	19	25.4	0.541	0.0504	28.12	389
25	60	2	650	19.5	19.48	0.7061	0.0584	24.42	240
26	60	6	650	19.5	30.75	0.4711	0.0412	38.75	533
27	60	2	750	19.5	20.45	0.6821	0.0558	21.38	358
28	20	6	650	18.5	28.07	0.5447	0.0462	34.74	457
29	40	4	700	19	25.21	0.536	0.0501	27.93	388
30	60	2	650	18.5	19.74	0.7347	0.0605	24.2	195
31	60	6	750	19.5	30.95	0.432	0.0377	35.42	648

Source: Authors, (2026).

The reduction of optimization trials is a subsequent advantage of RSM. Additional experimental trials are necessary for precise numerical validation of any approaches other than response surface methodology. The primary function of numerical models is to predict the behavior of input parameters and outcomes. The optimization method employs a higher-order polynomial equation to numerically model the nonlinear relationship between inputs and outputs. The subsequent equation denotes a second-order polynomial model [22].

$$Y = b_o + \sum b_i x_i + \sum b_{ij} x_i x_j (i, j = 1,2,3 \ldots \ldots k)$$

The variables Xi and Xj represent input variables, bi and bj denote constants, and Y signifies the output response. ANOVA was applied to analyze performance and emission parameters [23].

III.2.2 ANOVA results

Table 6: Analysis of variance for SFC and BTE.

Source	df	BTE		SFC	
		F-value	p-value	F-value	p-value
Model	10	16.91	< 0.0001	5.54	0.0007
A-Fuel	1	3.41	0.0805	0.5688	0.4600
B-Load	1	157.66	< 0.0001	44.33	< 0.0001
C-IP	1	0.4262	0.5217	2.09	0.1648
D-CR	1	0.0042	0.9491	0.2310	0.6363
AB	1	0.0333	0.8571	0.8454	0.3694
AC	1	0.0165	0.8990	0.1310	0.7214
AD	1	0.0172	0.8970	0.1535	0.6995
BC	1	0.0065	0.9365	0.0199	0.8893
BD	1	0.0164	0.8996	0.4177	0.5258
CD	1	0.0257	0.8744	1.49	0.2377
Residual	19				
Lack of Fit	11	240.96	< 0.0001	134.95	< 0.0001
Pure Error	8				
Cor Total	29				

Source: Authors, (2026).

Tables 6 and 7 present the findings of the analysis of variance (ANOVA) conducted on the experiments.

Table 7: Analysis of variance for $\boldsymbol{CO}, \boldsymbol{HC}$, and $\boldsymbol{NO_x}$ emission.

Source	DF	CO (%)		HC (ppm)		NO_x (ppm)	
		F-value	*p*-value	*F*-value	*p*-value	*F*-value	*p*-value
Model	10	17.41	< 0.0001	132.61	< 0.0001	51.38	< 0.0001
A-Fuel	1	6.86	0.0169	46.64	< 0.0001	2.75	0.1135
B-Load	1	151.15	< 0.0001	1098.49	< 0.0001	447.08	< 0.0001
C-IP	1	12.56	0.0022	49.01	< 0.0001	62.57	< 0.0001
D-CR	1	0.6844	0.4184	0.8237	0.3755	6.75	0.0176
AB	1	0.0059	0.9395	0.1518	0.7012	0.0895	0.7681
AC	1	0.1088	0.7452	0.3003	0.5901	0.0696	0.7948
AD	1	0.0001	0.9942	0.3942	0.5376	0.1028	0.7520
BC	1	0.1493	0.7035	0.1151	0.7381	0.0002	0.9901
BD	1	0.0005	0.9832	0.2271	0.6391	0.0084	0.9279
CD	1	0.0047	0.9461	0.0095	0.9232	0.0157	0.9016
Residual	19						
Lack of Fit	11	42.73	< 0.0001	17.79	0.0002	3.05	0.0622
Pure Error	8						
Cor Total	29						

Source: Authors, (2026).

A p-value below 0.01 signifies that the model is statistically significant. All models exhibit a p-value of less than 0.01. Consequently, ANOVA demonstrates that the model is statistically significant. The model F-values for SFC, BTE, CO, HC, and NOx are 390.07, 5.54, 16.91, 17.41, 132.61, and 51.38, respectively. The research indicated that nanoparticles and load substantially influence SFC (p-value <0.01). The suggested model and experimental variables can be evaluated using the P-value and F-value. Table 8 presents R2 values of 0.7445%, 0.8990%, 0.9016%, 0.9859%, and 0.9643% for SFC, BTE, CO, HC, and NOx, respectively, as indicated by the ANOVA results. The model's accuracy and adequacy are evidenced by the R2 value approaching 1. The R2 values indicate the efficacy of the models. The values of the Adjusted R2 (Adj. R2) and the Predicted R2 (Pred. R2) are relatively similar

Table 8: Model summary of input parameters.

Coefficient of determination	Value				
	BTE	SF	CO	HC	NO_x
R^2	0.8990	0.7445	0.9016	0.9859	0.9643
Adjusted R^2	0.8458	0.6100	0.8498	0.9784	0.9456
Predicted $\boldsymbol{R^2}$	0.7992	-0.0290	0.7910	0.9603	0.9340

Source: Authors, (2026).

IV. RESULT AND DISCUSSIONS

IV.1 ENGINE PERFORMANCE

IV.1.1 Specific fuel consumption (SFC)

Specific fuel consumption (SFC) refers to the amount of fuel burned per unit of time to provide a specified engine output. SFC is a quantitative measure for assessing an engine's efficacy in converting fuel into useable power. The initial equation is a second-order quadratic regression equation formulated to estimate SFC utilizing the coded values.

SFC = 0.573 -0.0200 A -0.1701B -0.0378 C -0.01248 D -0.0569 AB -0.02176 AC + 0.0232 AD -0.00908 BC + 0.0409 BD - 0.0798CD (1)

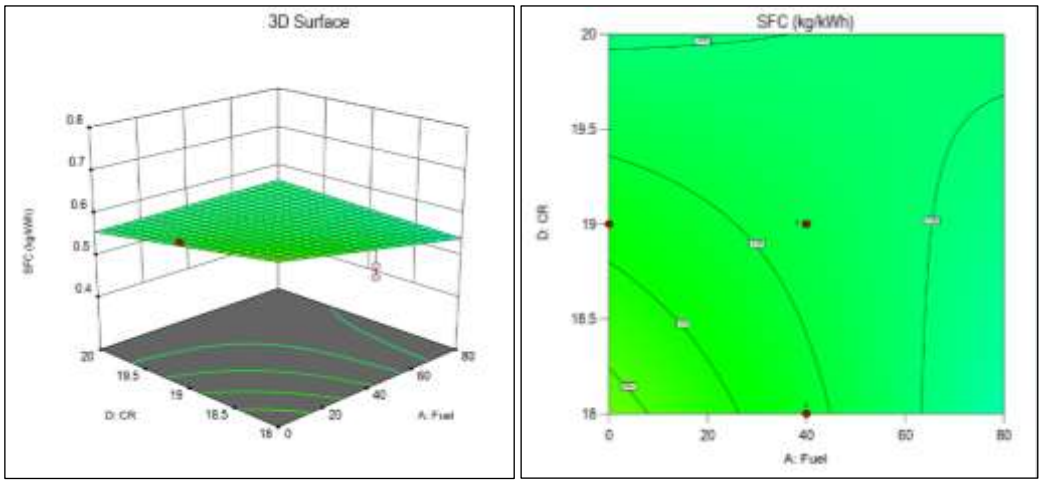

Figure 3: Three-dimensional plot depicts the impact of fuel and CR and their combined effect on the specific fuel consumption.
Source: Authors, (2026).

The influence of TiO_2 concentration in biodiesel and CR on SFC at IP (700 bar) and load (6 kg) was illustrated by contour and surface plots. At elevated CR, the light green hue of the contour zone yields a substantial concentration of nanoparticles (TiO_2) and a reduced engine specific fuel consumption (SFC). Biodiesel and CR exhibited a crimson hue with an escalating concentration of nanoparticles (TiO_2). As the TiO_2 to fuel ratio grew, the specific fuel consumption (SFC) value was found to decrease in figure 3. In another study, tested diesel–tomato seed oil biodiesel blends enhanced with nano-CuO (50 nm) additives in a single-cylinder engine. Nano-CuO improved fuel properties (flash/fire point, calorific value) and reduced SFC [24]. This is due to the fact that the expansion of nanoparticles improved the fuel's ignition characteristics by optimizing its air-fuel mixture, physicochemical properties (demonstrating increased fuel calorific value), dispersion, and thermal conductivity. A little reduction in SFC with increased CR indicates that enhanced combustion and diminished heat losses contributed to the overall decrease in SFC as CR increased. Under maximum load, the specific fuel consumption decreased by approximately 35% as the compression ratio increased from 18 to 20.

Figure 4 illustrates the effect of elevated injection pressure and compression ratio on specific fuel consumption (SFC) for a load of 4 kg and a fuel addition setting of 0. As IP increases, SFC diminishes with elevated CR. Decreased fuel usage results from increased spray pressure and a shorter duration for air/fuel combination. Figure 5, a contour plot depicts the influence of load and nano ratio on specific fuel usage. Figure 6 illustrates the trend of the specific fuel consumption curve in relation to the indicated power and fuel concentration, under a constant compression ratio and load. As the nanoparticle concentration and injection pressure increased, the contour plot indicates a drop in SFC. With a constant parameter load of 4 kg and CR, the SFC curve exhibits a slight increase or reduction contingent upon the IP level, as the nanoparticle concentration rises.

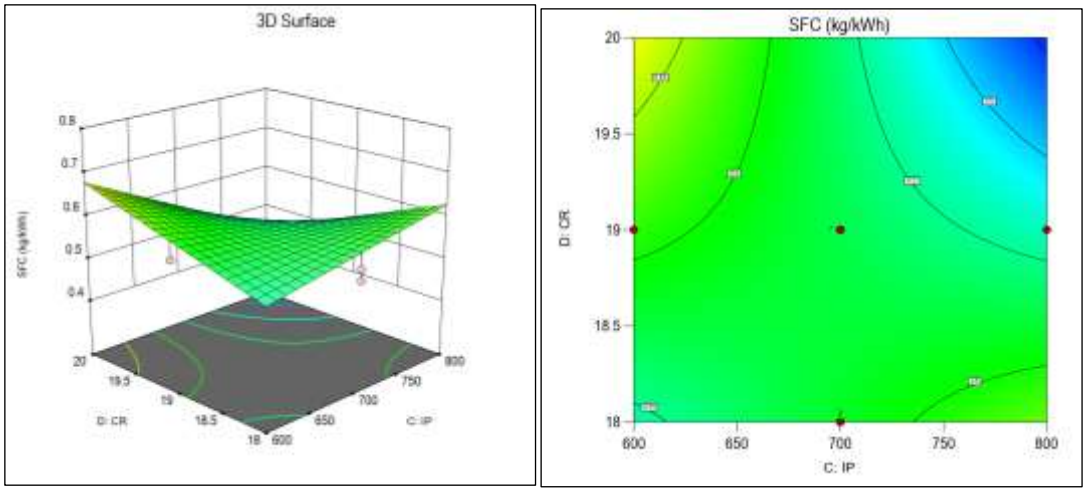

Figure 4: Three dimensional plot depicts the impact of IP and CR and their combined effect on the specific fuel consumption.
Source: Authors, (2026).

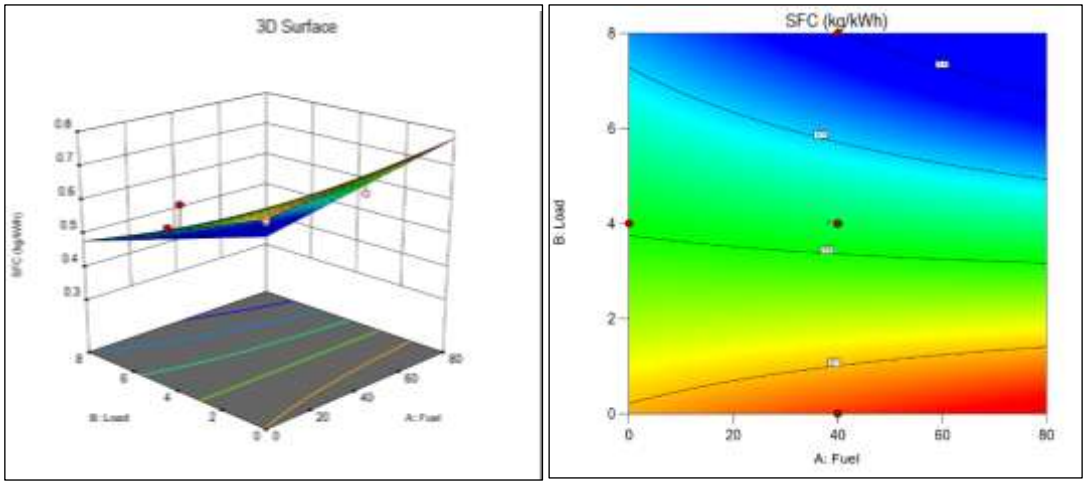

Figure 5: Three dimensional plot depicts the impact of fuel and load and their combined effect on the specific fuel consumption.
Source: Authors, (2026).

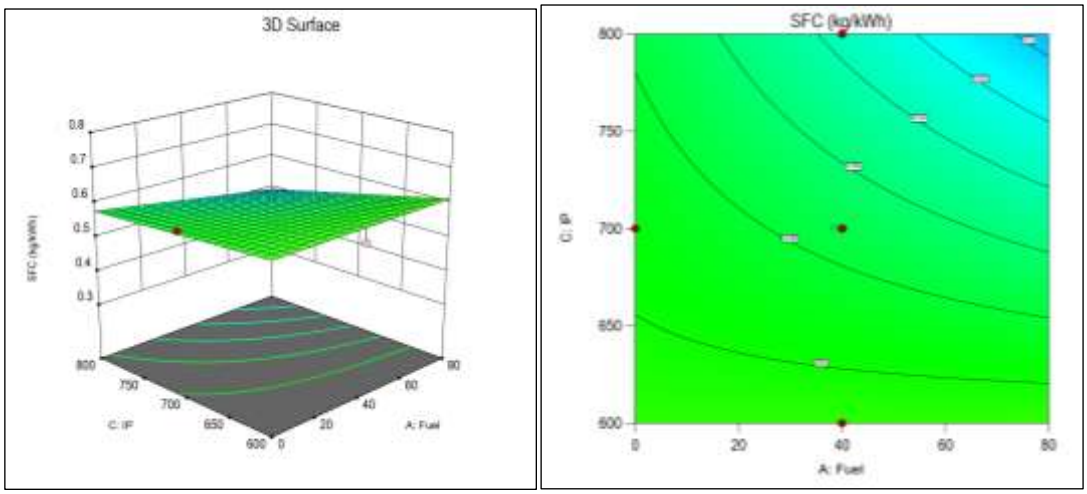

Figure 6: Three-dimensional plot depicts the impact of fuel and IP and their combined effect on the specific fuel consumption.
Source: Authors, (2026).

IV.1.2 Brake thermal efficiency (BTE)

To estimate BTE (utilizing the coded values), a second-order quadratic regression equation was formulated and denoted as equation (2).

BTE =24.23 + 1.744 A11 + .3809 B0 +.6056 C-0.0595 D0.+ 40084877135602 AB0.+.2742 AC0 +.27580 AD-0.1844 BC0.+ 28710 BD-0.3719 CD (2)

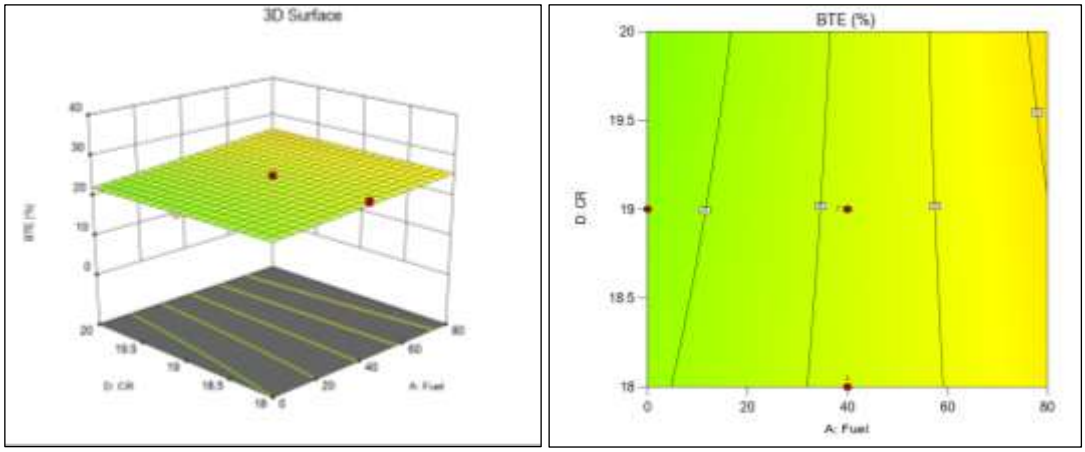

Figure 7: Three dimensional plot depicts the impact of fuel and CR and their combined impact on the brake thermal efficiency.
Source: Authors, (2026).

The Brake Thermal Efficiency (BTE) of the engine is a quantifiable indicator that assesses the engine's efficiency. Fuel conversion efficiency is the process of multiplying the lower heating value by the mass flow rate of injected fuel to produce energy. Using a load of 4 kg and an inlet pressure of 700 bar as fixed parameters, Figure 7 shows the contour and surface plot on the the influence of nanoparticle content and compression ratio on brake thermal efficiency. The addition of nanoparticles to biofuel resulted in an increased compression ratio and an elevated brake thermal efficiency curve. The utilization of nanoparticles signifies enhanced combustion and the effective transfer of fuel energy to productive labor. Optimal braking thermal efficiency was attained owing to the elevated heating value of the nano fuel and the substantial nanoparticle concentration within the fuel. An augmentation in BTE was seen with IP, as illustrated in Figure 8, demonstrating the impact of IP on BTE. Fuel injection transpires with reduced droplet sizes as the Fuel Injection Pressure (FIP) is elevated. This enhances the fuel's amalgamation with air and accelerates its vaporization. The combustion efficiency is improved, resulting in an increased brake thermal efficiency (BTE). In another study, lemongrass diesel engine tests showed B30ZnO had the highest BTE increase (>3%) and better emissions than TiO_2 or Al_2O_3 blends, with ANOVA confirming significant influence of nanoparticle type on performance [25].

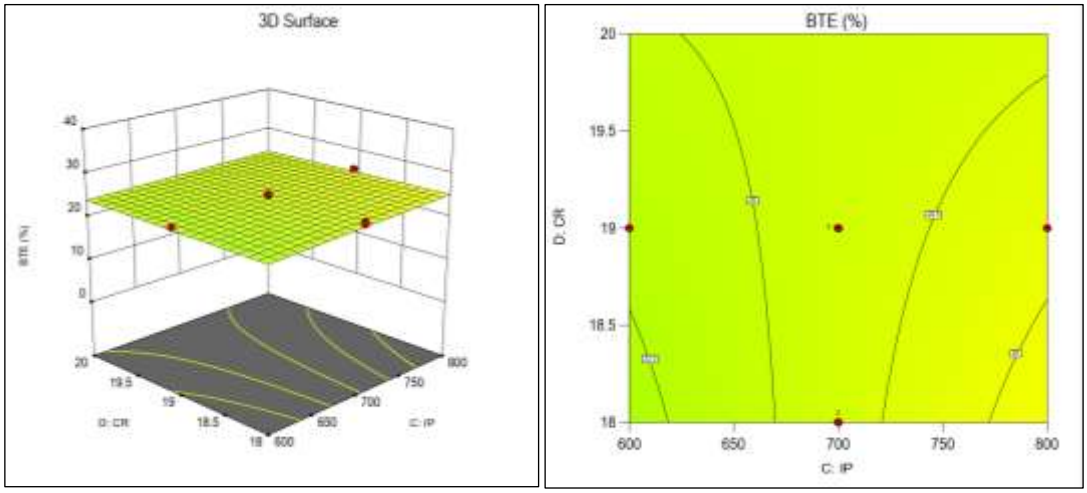

Figure 8: Three dimensional plot depicts the impact of IP and CR and their combined impact on the brake thermal efficiency.
Source: Authors, (2026).

Figure 9 illustrates the impact of load and nano fuel on BTE when the hold values are CR (19) and IP (700 bar). As the engine load intensified and the concentration of metallic nanoparticles augmented, its brake thermal efficiency enhanced. A minimal degree of heat loss is purported to enhance power as the load increases. Due to their elevated surface-to-volume ratio, nanoparticles facilitate the complete combustion of test fuel, hence enhancing brake thermal efficiency through nanoparticle advancement. Figure 10 illustrates the increase in BTE corresponding to the rising concentrations of IP and nanofuel. IP and nanoparticle enhancement improve fuel atomization, dispersion, and mixing, resulting in increased brake thermal efficiency.

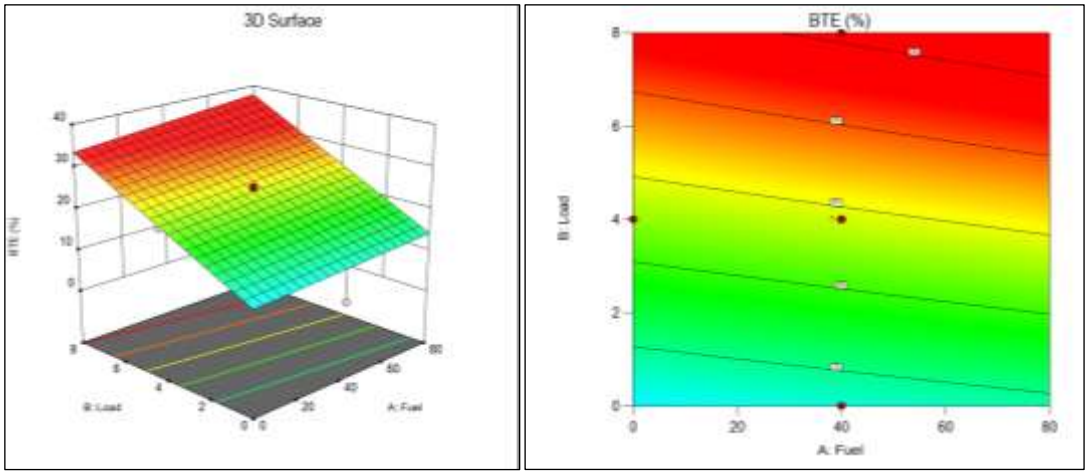

Figure 9: Three dimensional plot depicts the impact of fuel and load and their combined impact on the brake thermal efficiency.
Source: Authors, (2026).

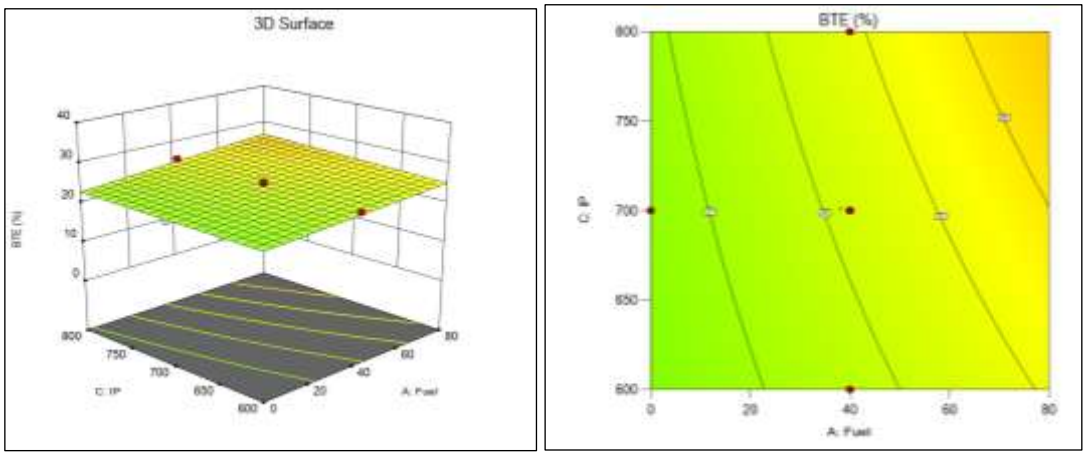

Figure 10: Three-dimensional plot depicts the impact of fuel and IP and their combined impact on the brake thermal efficiency.
Source: Authors, (2026).

IV.2 EMISSION CHARACTERISTICS

IV.2.1 CO emissions

The encoded values are utilized to formulate a second-order quadratic regression equation, employed to estimate CO as given in eqn (3).

$$CO = 0.05050 - 0.0035\,A - 0.0157\,B - 0.0046\,C - 0.0010\,D0 + .000239\,AB - 0.0009\,AC + 2.1932\text{-}05\,AD - 0.00125\,BC6 + 79151\text{-}05\,BD - 0.0002\,CD \quad (3)$$

Predictions for the response for specified levels of each element can be derived using the equation in terms of coded factors. The standard classification for the factors is +1 for elevated levels and -1 for diminished levels. To ascertain the relative significance of the factors, it is beneficial to compare their coefficients utilizing the coded equation.

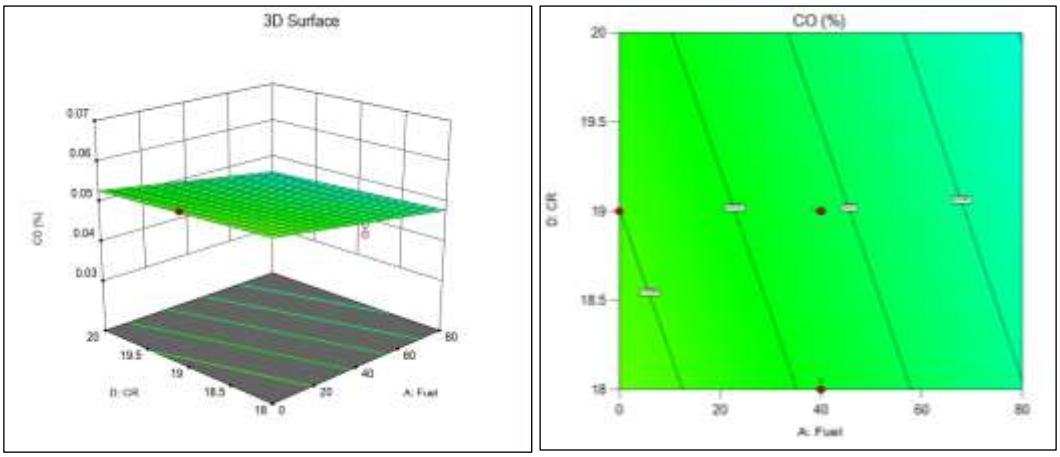

Figure 11: Three dimensional plot depicts the impact of fuel and CR and their combined impact on the CO emissions.
Source: Authors, (2026).

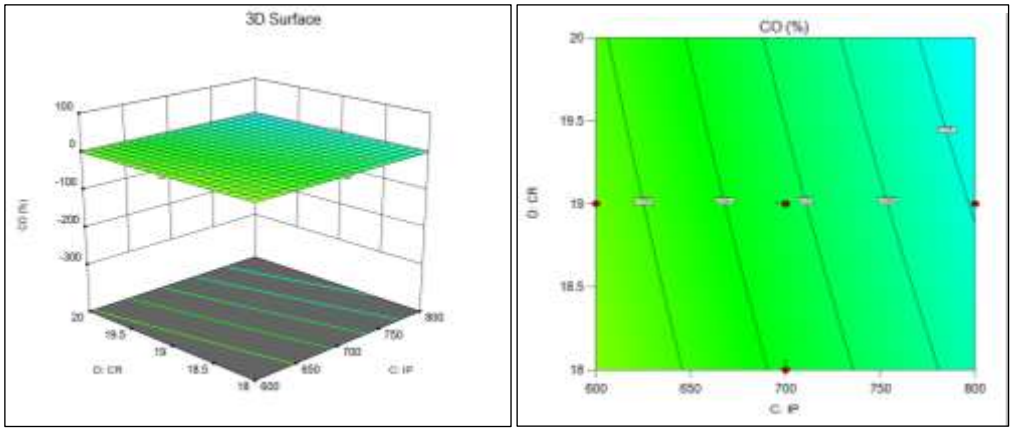

Figure 12: Three dimensional plot depicts the impact of IP and CR and their combined impact on the CO emissions.
Source: Authors, (2026).

The principal cause of carbon monoxide generation is the incomplete combustion of fuel. Figure 11 illustrates the changes in carbon monoxide for CR and nano fuel. The integration of nanoparticles reduced the carbon concentration due to complete burning. Metallic nanoparticles function as oxidation catalysts, transforming carbon monoxide into carbon dioxide during combustion. Metal nanoparticles also induced secondary atomization of the fuel. At elevated CR, the contour diagram indicated a decreased trend in CO emissions attributed to the augmented presence of nanoparticles. Figure 12's contour illustration depicts the impacts of CR and IP. In comparison to CR, IP exerts a more significant impact on CO emissions. To attain optimal air-fuel mixing, dispersion, penetration, and swirl ratio, the fuel was effectively atomized by elevating the injection pressure. CO emissions are significantly influenced by IP and CR. Figure 13 illustrates the significant impact of IP and nanoparticle concentration on CO emissions. The incorporation of nanoparticles into B25 lowers CO emissions. An optimal method to facilitate combustion is to augment the ratio of IP to nanoparticles. In another study, increasing tomato seed methyl ester content raised BTE, and NOx but reduced CO, smoke, and HC emissions across loads. TSME–n-butanol–diesel blends offer favorable emission and performance trade-offs [26]. Figure 14 illustrates the variation in CO with respect to load and TiO_2 content. As the load increases, both combustion temperature and pressure elevate, resulting in a higher ignition flame temperature and, consequently, enhanced combustion efficiency.

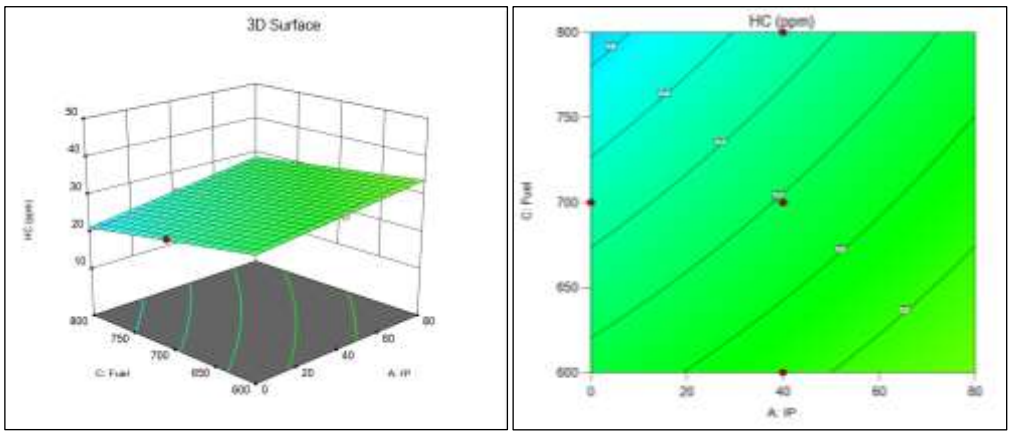

Figure 13: Three dimensional plot depicts the impact of IP and fuel and their combined impact on the CO emissions.
Source: Authors, (2026).

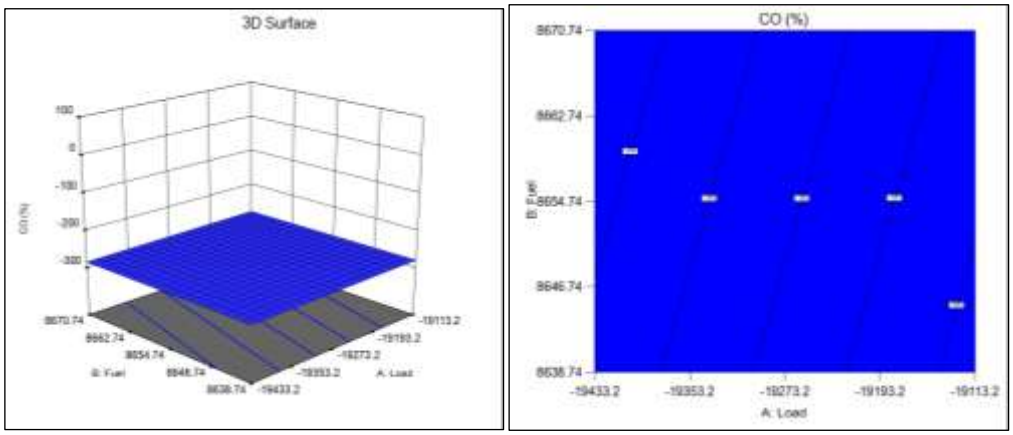

Figure 14: Three dimensional plot depicts the impact of load and fuel and their combined impact on the CO emissions.
Source: Authors, (2026).

IV.2.2 HC emissions

A second-order quadratic regression equation was created to estimate HC (utilizing the coded values), represented by equation (4).

$$HC = 28.16826\ 3.16471\ A14.+\ 73017\ B - 3.18461C0.4099\ D - 0.4195AB + 0.57291\ AC0.+\ 64735\ AD0 + .3800\ BC0.+\ 52447 + BD\text{-}0.1111\ CD \quad (4)$$

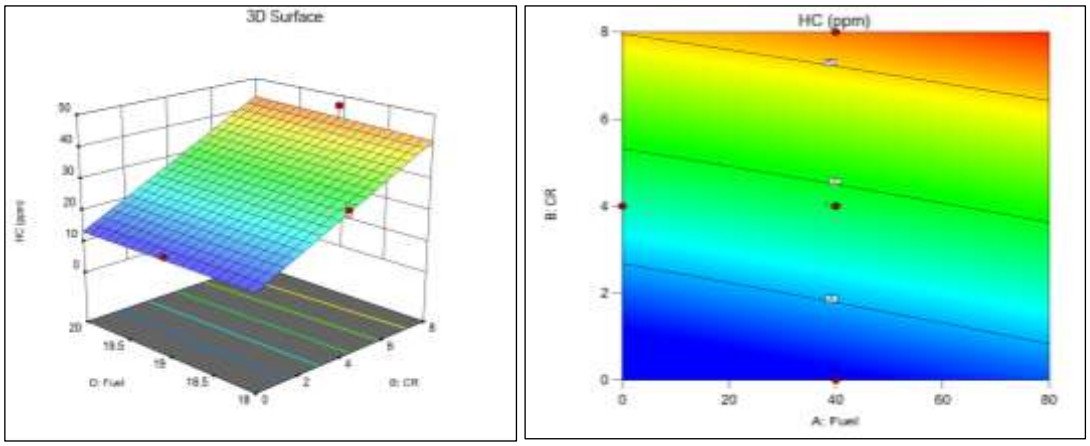

Figure 15: Three dimensional plot depicts the impact of CR and fuel and their combined impact on the HC emissions.
Source: Authors, (2026).

Elevated HC emissions result from incomplete combustion of fuel particles. At which load (4 kg) and pressure (700 bar) do the different nanoparticle concentrations in B25 and CR exhibit as HC. The outcomes are illustrated in Figure 15. Researchers found that augmenting the nanoparticle ratio resulted in a little increase in HC emissions. The large specific heat capacity of the nanoparticle is likely due to the unburned fraction of the charge being simulated. In comparison to alternative test fuels, biodiesel generated reduced hydrocarbon emissions, likely attributable to enhanced fuel ignition resulting from the elevated oxygen content in biofuel molecules. Figure 16 shows the impact of engine load and biodiesel nanoparticle ratio on hydrocarbon emissions. The presence of nanoparticles in biodiesel reduced the activation temperature of carbon and enhanced ignition, hence diminishing hydrocarbon emissions.

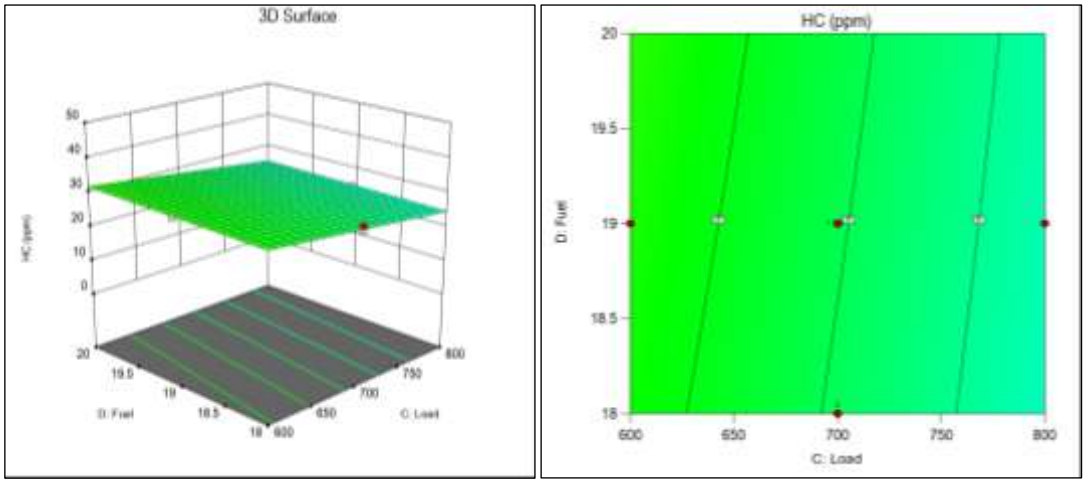

Figure 16: Three dimensional plot depicts the impact of load and fuel and their combined impact on the HC emissions.
Source: Authors, (2026).

The decrease in HC is attributed to improved fuel combustion resulting from increased IP, which facilitates optimal fuel atomization and reduces fuel droplet evaporation. Elevated compression ratios lowered HC emissions, which is advantageous for CR. An elevation in CR resulted in an increase in temperature, pressure, and flame velocity within the cylinder. Figure 17 indicated that HC emissions were reduced with increasing CR and IP. Due to the diminished flame speed during fuel ignition, flame quenching and insufficient ignition may elevate hydrocarbon levels. At elevated IP and CR, HC discharge diminished, as illustrated in Figure 17. Figure 18 illustrates the HC discharge with IP and fuel, with hold values recorded as CR (19) and load (4 kg). Consequently, an unforeseen reduction in HC levels was observed at elevated IP for the optimal nano ratio fuel ignition. A higher engine IP and biodiesel with increased nanoparticle content are effective parameters for reducing HC discharges. In another study, TiO_2 nanoparticle evaluated on Pongamia pinnata biodiesel in a single-cylinder diesel engine. TiO_2 addition improved BTE by 1.72% and BSFC by 3.57% compared to biodiesel alone, and reduced CO, HC, and NOx emissions, attributed to better atomization and oxidation from nanoparticle oxygen content [27].

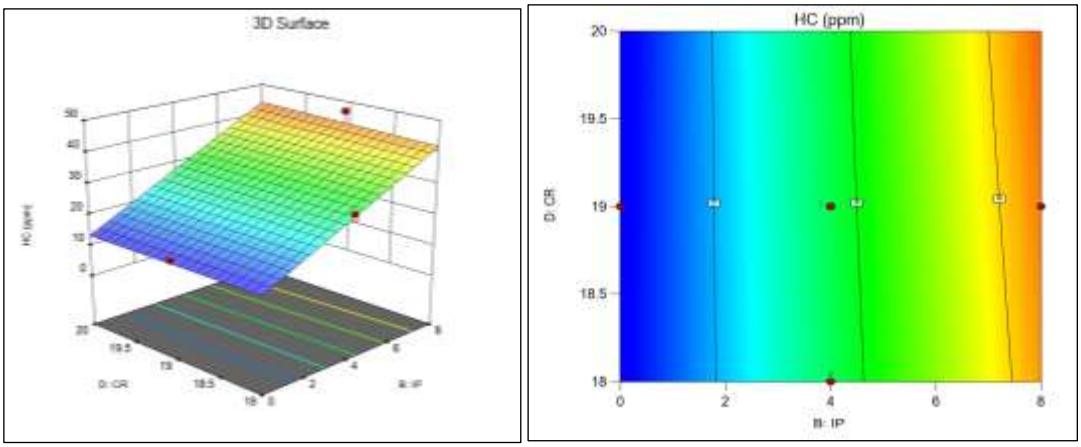

Figure 17: Three dimensional plot depicts the impact of CR and IP and their combined impact on the HC emissions.
Source: Authors, (2026).

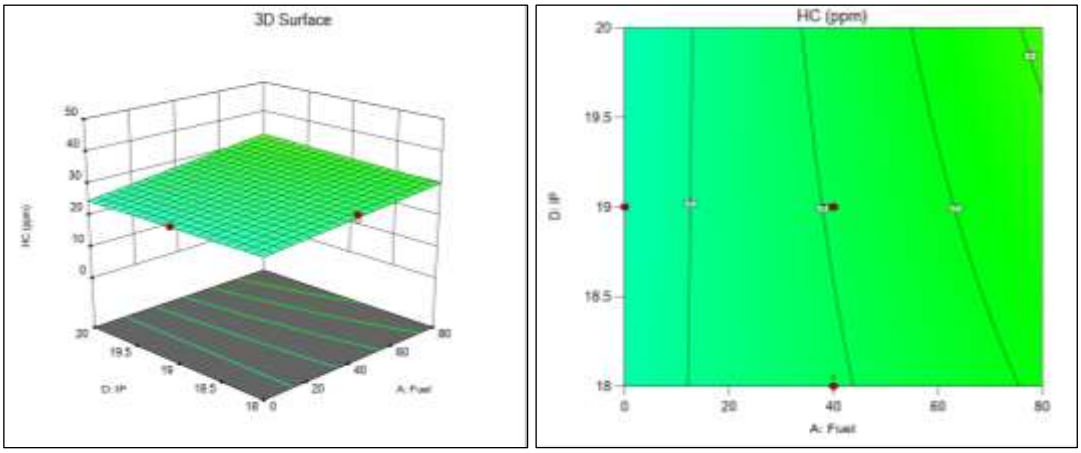

Figure 18: Three dimensional plot depicts the impact of fuel and IP and their combined impact on the HC emissions.
Source: Authors, (2026).

IV.2.3 NOx emissions

The result of the NOX estimation procedure is Equation (5), a second-order quadratic regression equation utilizing the coded values.

$$NOx = 409.8483\ 24.035\ A293 + .7823\ B112 + 4863\ C36 + .6979\ D10 + 0723\ AB8 + 6214\ AC10 + 33490\ AD0 + 43936\ BC3 + 1528\ BD - 4.4590\ CD \quad (5)$$

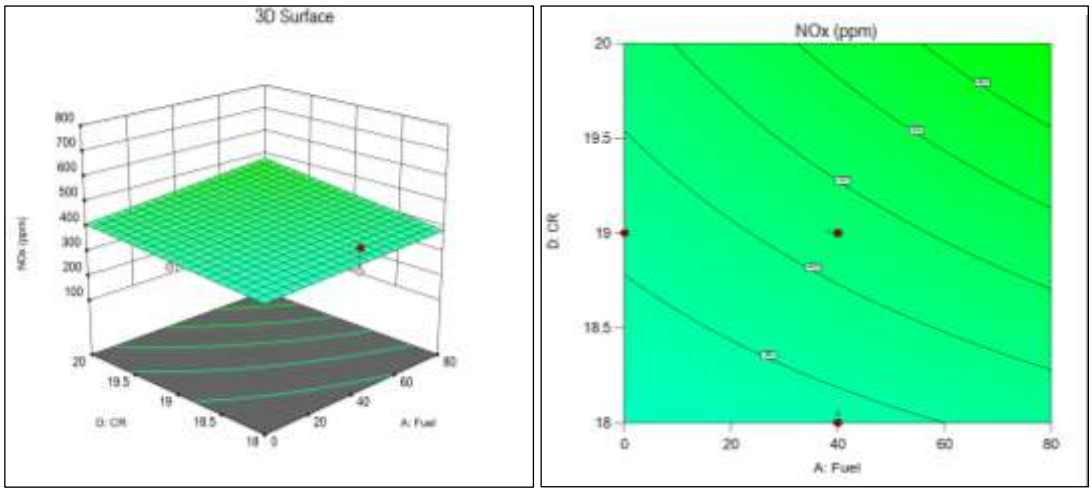

Figure 19: Three dimensional plot depicts the impact of fuel and CR and their combined impact on NOx emissions.
Source: Authors, (2026).

The combustion of biodiesel at elevated temperatures generates significant quantities of nitrogen oxides (NOx) due to its increased oxygen content. Figure 19 illustrates nitrogen oxide emissions associated with nano biofuel and CR. The rise in NOx emissions with CR may be due to elevated in-cylinder combustion pressure and temperature. Figure 20 illustrates that withhold values of load (4 kg) and injection pressure (700 bar), NOx emissions escalate at elevated compression ratios.

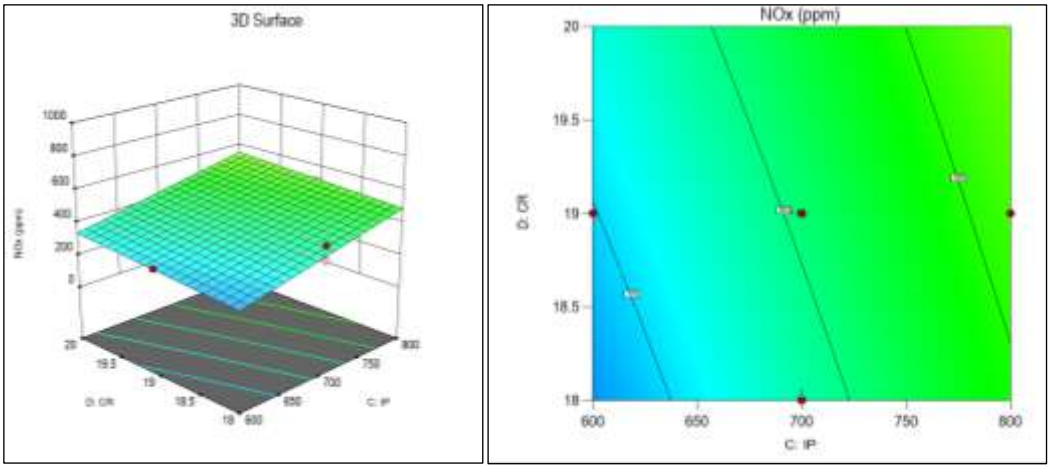

Figure 20: Three dimensional plot depicts the impact of IP and CR and their combined impact on NOx.
Source: Authors, (2026).

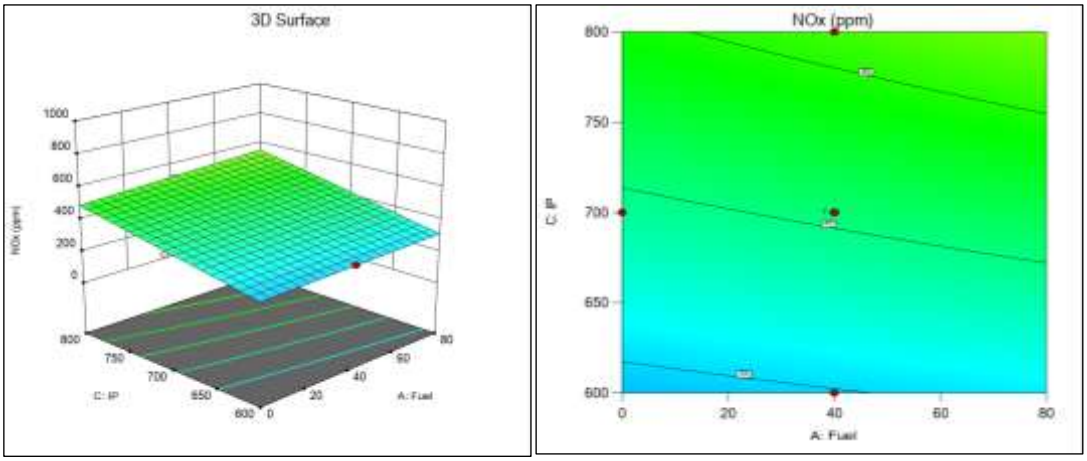

Figure 21: Three dimensional plot depicts the impact of fuel and IP and their combined impact on NOx emissions.
Source: Authors, (2026).

The contour figure indicates that increases in engine load and compression ratio corresponded with elevated NOx emissions. Figure 21 illustrates the variation of NOx emissions in relation to nano fuel and load. Figure 22 illustrates the variation of NOx emissions with varying injection pressures and nanoparticle concentrations in B25. In comparison to B25, the TiO_2 fuel blend exhibited elevated NOx emissions. Oxygenated nanoparticles improve combustion and reduce the ignition delay, since a higher ratio of nanoparticles facilitates rapid premixed ignition, elevates the burning temperature, and increases NOx emissions. In previous study, 20% *Chlorella* biodiesel blends compared with TiO_2 nanoparticle enhancements (50–150 ppm) at CRs 17–18. The D80CvBD20$TiO_2$100 blend achieved peak CP of 63.45 bar at CR 18 and reduced unburnt hydrocarbons by up to 13%. TiO_2 increased NOx but reduced CO due to higher combustion temperatures and oxygen availability [28].

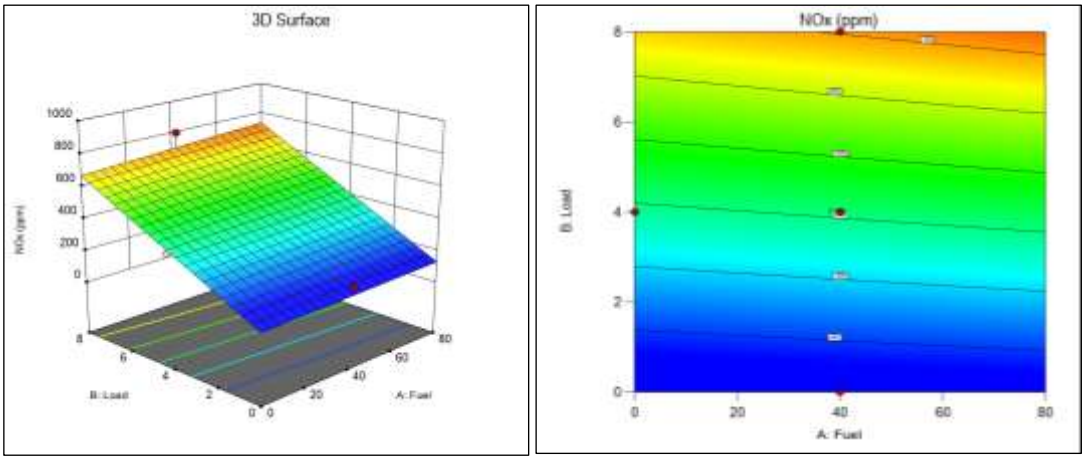

Figure 22: Three-dimensional plot depicts the impact of fuel and load and their combined impact on NOx.
Source: Authors, (2026).

Table 9: Comparative analysis of engine at optimized value.

Best value under the RSM optimization method									
Optimization method	**The best composition of the fuel**	**Engine operating parameter**			**Engine performance parameter**		**Engine emissions**		
		IP (bar)	**CR**	**Load (kg)**	**BTE (%)**	**SFC kJ/kg.hr**	**CO (%)**	**HC (ppm)**	**NO_x (ppm)**
RSM	50.47	799	20	3.63	023.96	0.45	0.044	25.03	538
The experimental result at the optimum parameter investigated by RSM									
Engine	**Composition of fuel**	**IP (bar)**	**CR**	**Load (kg)**	**BTE (%)**	**SFC kJ/kg.hr**	**CO (%)**	**HC (ppm)**	**NO_X (ppm)**
VCR CRDI engine	49.47	789	18	2.83	22.46	0.25	0.023	22.01	536
Comparative analysis between optimization result and experimental result									
Engine responses	**BTE (%)**	**SFC kJ/kg.hr**			**CO (%)**	**HC (ppm)**	**NO_x (ppm)**		
%Error	6.2	44.4			47.72	12.06	0.37		

Source: Authors, (2026).

V. CONCLUSION

This study examines the impact of various engine operating parameters on performance metrics (BTE and SFC) and emissions (CO, HC, and NOX). The parameters being examined are load, IP, CR, and the concentration of nanoparticles in biodiesel. The responses of the CRDI VCR diesel engine are optimized for each engine input parameter through response surface approach. A numerical model was developed to analyze the BTE, BSFC, CO, HC, and NOx emissions from the engine. Findings from optimization and variance analysis indicate that RSM is an effective method for refining diesel engine performance across various input parameters. The calculated R^2 values for BTE, SFC, CO, HC, and NOX emissions are 0.8990, 0.7445, 0.9016, 0.9859, and 0.9643, respectively. These figures can be accepted with confidence. The ideal input engine parameter, found by RSM, is a 50.47 nanoparticle/B25/CR/790.9 bar IP mixture operating at a 3.63 kg engine load. Moreover, for the most thoroughly examined engine inputs, the optimal values of BTE, SFC, CO, HC, and NOX are 22.46%, 0.25 kg/kWh, 23%, 22.01 ppm, and 536 ppm, respectively. Consequently, the model possesses a robust statistical base. Experimental trials indicate that errors fall within an acceptable range, and comparative analysis of RSM optimizes value. Thus, engine performance and emissions can be improved by employing the ideal value. This study's results indicate that biodiesel augmented with TiO_2 nanoparticles may serve as a cleaner and more efficient alternative fuel for engines.

VI. AUTHOR'S CONTRIBUTION

Conceptualization: Kumaran P, Sathiyaraj S
Methodology: Kumaran P and Sathiyaraj S
Investigation: Easkki Mani K and Albin Raj.
Discussion of results: Kumaran P, Sathiyaraj S and Vijayakumar K.
Writing – Original Draft: Kumaran P
Writing – Review and Editing: Sathiyaraj S and Vijayakumar K.
Resources: Kumaran P
Supervision: Sathiyaraj S and Vijayakumar K.
Approval of the final text: Kumaran P, Sathiyaraj S and Vijayakumar K.

VII. REFERENCES

[1] F. Markić, K. Kraljić, V. Stulić, S. Pleslić, T. V Pavičić, and N. Maltar-Strmečki, "Improving the extraction of tomato seed oil and the retention of bioactive substances using pulsed electric field technology," Future Foods, vol. 12, 2025, doi: 10.1016/j.fufo.2025.100706.

[2] P. Squillace, F. Adani, and B. Scaglia, "Supercritical CO2 extraction of tomato pomace: Evaluation of the solubility of lycopene in tomato oil as limiting factor of the process performance," Food Chem, vol. 315, 2020, doi: 10.1016/j.foodchem.2020.126224.

[3] K. Sangeetha, R. B. Ramyaa, A. Mousavi Khaneghah, and M. Radhakrishnan, "Extraction, characterization, and application of tomato seed oil in the food industry: An updated review," J Agric Food Res, vol. 11, 2023, doi: 10.1016/j.jafr.2023.100529.

[4] I. Solaberrieta, A. C. Mellinas, J. Espagnol, M. Hamzaoui, A. Jiménez, and M. C. Garrigós, "Valorization of Tomato Seed By-Products as a Source of Fatty Acids and Bioactive Compounds by Using Advanced Extraction Techniques," Foods, vol. 11, no. 16, 2022, doi: 10.3390/foods11162408.

[5] R. Karami, M. G. Rasul, and M. M. K. Khan, "An Empirical and Computational Fluid Dynamics Analysis of Combustion Performance of a Diesel Engine Fueled With Tomato Seed Oil Biodiesel," Journal of Energy Resources Technology, Transactions of the ASME, vol. 145, no. 4, 2023, doi: 10.1115/1.4055470.

[6] D. P. Rao et al., "Adsorptive removal of cadmium from electroplating wastewater using hybrid composite of thiol-grafted seed gum of Tamarindus indica and Teff hay biocarbon," Zeitschrift fur Physikalische Chemie, vol. 239, no. 5, pp. 633–654, 2025, doi: 10.1515/zpch-2024-0715.

[7] B. Gaddala et al., "Evaluation of detoxification performance of Pithecellobium dulce seed pod powder upon acid treatment: removal of reactive red 195-A dye and kinetic analysis," Zeitschrift fur Physikalische Chemie, vol. 239, no. 6, pp. 885–910, 2025, doi: 10.1515/zpch-2024-0879.

[8] T. Ouatmani, H. Haddadi-Guemghar, L. Boulekbache-Makhlouf, D. Mehidi-Terki, A. Maouche, and K. Madani, "A sustainable valorization of industrial tomato seeds (cv Rio Grande): Sequential recovery of a valuable oil and optimized extraction of antioxidants by microwaves," J Food Process Preserv, vol. 46, no. 1, 2022, doi:

10.1111/jfpp.16123.

[9] P. Kumaran, S. Natarajan, R. Shanmuga Raj, S. Dhanaraj, and V. R. Kumar, “Performance and emissions on VCR diesel engine with turbocharger setup running using tomato seed oil,” in Materials Today: Proceedings, 2020, pp. 6078–6082. doi: 10.1016/j.matpr.2020.10.080.

[10] P. Kumaran, S. Natarajan, M. Maheshwaran, K. Rizal, and B. C. Rohith, “Investigation on Performance and Emission Characteristics of VCR Diesel Engine with Different Nozzles Using Blends of Tomato Seed Oil,” in AIP Conference Proceedings, 2023. doi: 10.1063/5.0110969.

[11] H. A. Mahmood, A. O. Al-Sulttani, H. A. Alrazen, and O. H. Attia, “The impact of different compression ratios on emissions, and combustion characteristics of a biodiesel engine,” AIMS Energy, vol. 12, no. 5, pp. 924–945, 2024, doi: 10.3934/ENERGY.2024043.

[12] M. Kiralan and O. Ketenoglu, “Utilization of Tomato (Solanum lycopersicum) by-Products: An Overview,” in Mediterranean Fruits Bio-wastes: Chemistry, Functionality and Technological Applications, 2022, pp. 799–818. doi: 10.1007/978-3-030-84436-3_34.

[13] M. Casa, C. Prizio, and M. Miccio, “Biodiesel production from tomato seed by transesterification with Alkaline and ‘Green’ catalysts: Simulation and discussion,” Chem Eng Trans, vol. 87, pp. 451–456, 2021, doi: 10.3303/CET2187076.

[14] R. Karami, M. G. Rasul, M. M. K. Khan, and M. Mahdi Salahi, “Experimental and computational analysis of combustion characteristics of a diesel engine fueled with diesel-tomato seed oil biodiesel blends,” Fuel, vol. 285, 2021, doi: 10.1016/j.fuel.2020.119243.

[15] V. H. Özyurt, I. Tetik, and S. Ötleş, “Influence of process conditions on ultrasound-assisted protein extraction from cold pressed tomato seed waste,” J Food Process Preserv, vol. 45, no. 12, 2021, doi: 10.1111/jfpp.16079.

[16] V. H. Ozyurt, B. Çakaloğlu, and S. Otles, “Optimization of cold press and enzymatic-assisted aqueous oil extraction from tomato seed by response surface methodology: Effect on quality characteristics,” J Food Process Preserv, vol. 45, no. 5, 2021, doi: 10.1111/jfpp.15471.

[17] B. Maleki, H. Esmaeili, M. Mansouri, D. Kumar, and B. Singh, “Enhanced conversion of dairy waste oil to biodiesel via novel and highly reactive UiO-66-NH2/ZnO/TiO2 nano-catalyst: Optimization, kinetic, thermodynamic and diesel engine studies,” Fuel, vol. 339, 2023, doi: 10.1016/j.fuel.2022.126901.

[18] S. Muniyappan and R. Krishnaiah, “Experimental and artificial neural network (ANN) study on the impact of three different metal oxide nanoparticle combustion enhancers enriched on mahua biodiesel-diesel fuelled CI engine,” Engineering Research Express, vol. 6, no. 4, 2024, doi: 10.1088/2631-8695/ad9984.

[19] S. Muniyappan and R. Krishnaiah, “The influence of TiO2 nanoparticles on the performance, combustion, and emissions on ternary blends of n-heptane, mahua biodiesel and diesel-fuelled engine using response surface methodology,” Case Studies in Chemical and Environmental Engineering, vol. 10, 2024, doi: 10.1016/j.cscee.2024.100900.

[20] X. Zhang, “RSM-based optimization for ultrasound-assisted transesterification of Jojoba oil to biodiesel via ZnFe2O4@TiO2 retrievable nanocatalyst: Application on the diesel engine,” Ind Crops Prod, vol. 220, 2024, doi: 10.1016/j.indcrop.2024.119144.

[21] P. Sujin, S. S. Selva Roji, A. J. Kings, and L. R. M. Miriam, “Optimization of engine performance, emission and combustion parameters by using mixed nonedible oil biodiesel with nano-additives using hybrid techniques,” Energy, vol. 305, 2024, doi: 10.1016/j.energy.2024.132413.

[22] A. P. Edlabadkar et al., “Optimization of Mechanical Properties of Cordia dichotoma/Alumina Nanoparticle Reinforced Epoxy Nanocomposites Under Alkali Treatment Using ANN Techniques,” Journal of Environmental Nanotechnology, vol. 14, no. 2, pp. 525–540, 2025, doi: 10.13074/jent.2025.06.2521549.

[23] R. Karami, M. G. Rasul, and M. M. K. Khan, “CFD simulation and a pragmatic analysis of performance and emissions of tomato seed biodiesel blends in a 4-cylinder diesel engine,” Energies (Basel), vol. 13, no. 14, 2020, doi: 10.3390/en13143688.

[24] K. Lenin, S. Raghuvaran, K. B. Hariharan, M. Manimaran, H. Ramakrishnan, and S. Dhanabalan, “Experimental investigation on single cylinder four-stroke diesel engine with copper oxide nano-additives using tomato seed oil,” in Materials Today: Proceedings, 2022, pp. 1280–1291. doi: 10.1016/j.matpr.2022.08.401.

[25] M. Sunil Kumar, R. Rajasekar, S. Ganesan, S. P. Venkatesan, and V. Praveen Kumar, “Evaluation of metal oxide nano particles in lemongrass biodiesel for engine performance, emission and combustion characteristics,” in Materials Today: Proceedings, 2021, pp. 3657–3665. doi: 10.1016/j.matpr.2020.10.796.

[26] H. Sivasubramanian, V. Sundaresan, S. K. Ramasubramaniam, S. R. Shanmugaiah, and S. K. Nagarajan, “Investigation of biodiesel obtained from tomato seed as a potential fuel alternative in a CI engine,” Biofuels, vol. 11, no. 1, pp. 57–65, 2020, doi: 10.1080/17597269.2017.1338124.

[27] M. K. Parida, P. Mohapatra, S. S. Patro, and S. Dash, “Effect of TiO2 nano-additive on performance and emission characteristics of direct injection compression ignition engine fueled with Karanja biodiesel blend,” Energy Sources, Part A: Recovery, Utilization and Environmental Effects, vol. 46, no. 1, pp. 7521–7530, 2024, doi: 10.1080/15567036.2020.1756991.

[28] V. Hariram et al., “Influence of TiO2 Nanoparticles on Engine Parameters at Varied Compression Ratio of CI Engine Fuelled with Biodiesel,” Journal of Environmental Nanotechnology, vol. 14, no. 2, pp. 58–68, 2025, doi: 10.13074/jent.2025.06.2511378.